18. Harada, M. & Suguri, S. Surveys on cercariae in brackish water snails in Kagawa Prefecture, Shikoku, Japan. *Jpn. J. Parasitol.* **38,** 388–391 (1989).
19. Chapman, F. M. *Handbook of Birds from Eastern North America* (Dover, New York, 1966).
20. Hair, J. D. & Forrester, D. J. The helminth parasites of the starling (*Sturnus vulgaris* L.): A checklist and analysis. *Am. Midl. Nat.* **83,** 555–564 (1970).
21. Mitchell, C. E. & Power, A. G. Release of invasive plants from fungal and viral pathogens. *Nature* this issue.
22. Gregory, R. D. & Blackburn, T. M. Parasite prevalence and host sample size. *Parasitol. Today* **7,** 316–318 (1991).

Supplementary Information accompanies the paper on *Nature*'s website (http://www.nature.com/nature).

Acknowledgements This work was conducted as part of the Diseases and Conservation Biology Working Group supported by the National Center for Ecological Analysis and Synthesis, a centre funded by the National Science Foundation (NSF), the University of California, and the Santa Barbara campus. We thank S. Altizer, S. Gaines, P. Hudson, H. McCallum, A. W. Miller, C. Mitchell and A. Power for discussion and comments; A. Dove and G. Ruiz for providing data; and L. Mababa for data collection. This research was supported by NSF through the NIH/NSF Ecology of Infectious Disease Program, and by the National Sea Grant College Program, National Oceanic and Atmospheric Administration (NOAA), US Department of Commerce through the California Sea Grant College System, and in part by the California State Resources Agency. The views expressed herein are those of the authors and do not necessarily reflect the views of NOAA or any of its subagencies. The US Government is authorized to reproduce and distribute for governmental purposes.

Competing interests statement The authors declare that they have no competing financial interests.

Correspondence and requests for materials should be addressed to M.E.T. (e-mail: torchin@lifesci.ucsb.edu).

The contribution of *Shaker* K^+ channels to the information capacity of *Drosophila* photoreceptors

Jeremy E. Niven*†, Mikko Vähäsöyrinki†‡, Mika Kauranen‡, Roger C. Hardie§, Mikko Juusola* & Matti Weckström‡

** Physiological Laboratory, University of Cambridge, Cambridge CB2 3EG, UK*
‡ Department of Physical Sciences, Division of Biophysics, University of Oulu, PO Box 3000, 90014 Oulun Yliopisto, Oulu, Finland
§ Department of Anatomy, University of Cambridge, Cambridge CB2 3DY, UK
† These authors contributed equally to this work

An array of rapidly inactivating voltage-gated K^+ channels is distributed throughout the nervous systems of vertebrates and invertebrates[1–5]. Although these channels are thought to regulate the excitability of neurons by attenuating voltage signals, their specific functions are often poorly understood. We studied the role of the prototypical inactivating K^+ conductance, *Shaker*[6,7], in *Drosophila* photoreceptors[8,9] by recording intracellularly from wild-type and *Shaker* mutant photoreceptors. Here we show that loss of the *Shaker* K^+ conductance produces a marked reduction in the signal-to-noise ratio of photoreceptors, generating a 50% decrease in the information capacity of these cells in fully light-adapted conditions. By combining experiments with modelling, we show that the inactivation of *Shaker* K^+ channels amplifies voltage signals and enables photoreceptors to use their voltage range more effectively. Loss of the *Shaker* conductance attenuated the voltage signal and induced a compensatory decrease in impedance. Our results demonstrate the importance of the *Shaker* K^+ conductance for neural coding precision and as a mechanism for selectively amplifying graded signals in neurons, and highlight the effect of compensatory mechanisms on neuronal information processing.

Insect photoreceptors have provided a model system for examining specific molecular mechanisms involved in information processing with graded voltage signals, including signal transduction (the phototransduction cascade)[10] and membrane filtering (the photo-insensitive membrane)[11]. Using these mechanisms, insect photoreceptors must compress the vast spatiotemporal range of light intensities to which they are exposed into voltage responses of limited amplitude and speed. In *Drosophila*, these mechanisms can be studied in relative isolation by patch-clamping dissociated photoreceptors, but *in vitro* photoreceptors do not survive prolonged light stimulation. By contrast, *in vivo* photoreceptors can be recorded intracellularly for more than an hour, and exposed to a full range of light intensities[12] (Fig. 1a). The photo-insensitive membrane of these cells contains three voltage-activated K^+ channels: a *Shaker* channel that generates an A-type current, a slow delayed rectifier and, in some cells, a fast delayed rectifier[9]. The contribution of the *Shaker* K^+ channel and its functional homologues (including vertebrate Kv channels)[2,3] to neuronal function remains unclear, although they are thought to attenuate the amplitude of graded potentials and back-propagated action potentials in dendrites[13–15], to influence the firing frequency of spiking neurons[16] and to determine the reliability of spike propagation[17]. The performance of a photoreceptor in coding a light signal can be described quantitatively by its sensitivity, signal-to-noise ratio and frequency response, allowing specific components of the signalling machinery, including ion channels, to be related to specific aspects of cellular

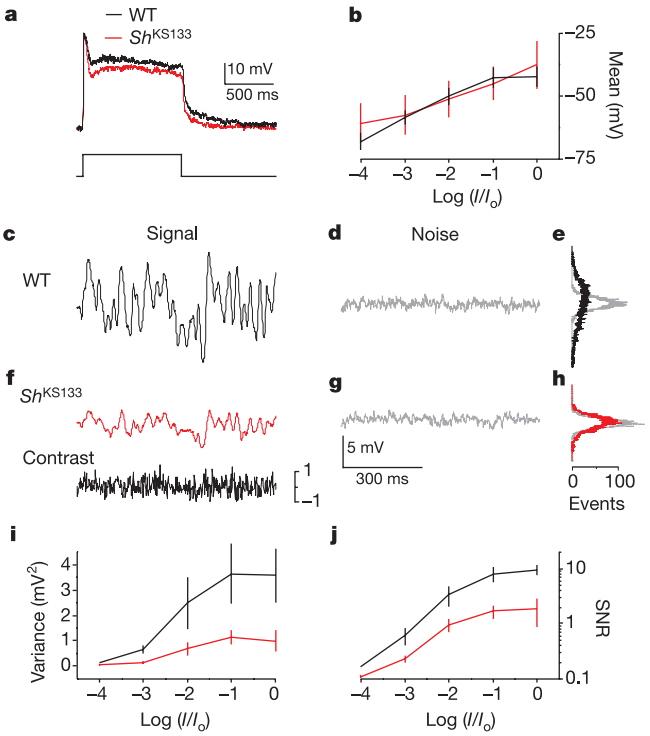

Figure 1 *Shaker* K^+ channels amplify photoreceptor voltage responses. **a**, Responses of wild-type (WT, black) and *Sh*^{KS133} (red) photoreceptors to a 1 s pulse of light. **b**, Mean (±s.e.m.) depolarization of WT (black) and *Sh*^{KS133} (red) photoreceptors to dynamically modulated light contrast at five light intensities ($n = 6$ for each photoreceptor type in all experiments presented here). I, given background light intensity; I_0, maximum background light intensity. **c**, **f**, Waveform of the average voltage signal of WT (black) and *Sh*^{KS133} (red) photoreceptors to noise-modulated light contrast at the highest light intensity. **d**, **g**, Corresponding voltage noise (grey) for the averages presented in **c** and **f**. **e**, **h**, Distributions of the signal (WT, black; *Sh*^{KS133}, red) and noise (grey) for **c**–**g**. **i**, **j**, The signal variance (**i**) and the signal-to-noise ratio (SNR, **j**) for WT (black) and *Sh*^{KS133} (red) photoreceptors at each adapting-light background.

function[11]. The information capacity of the photoreceptors, a measure of the number of states a signalling system can transmit in a given time window, can also be calculated from the signal-to-noise ratio[18]. We used these quantitative measures, combined with a mathematical model of the photoreceptors, to assess the contribution of the *Shaker* K^+ conductance to photoreceptor performance.

The signalling efficiency of photoreceptors in wild-type (WT) flies and Sh^{KS133} flies[7], which produce non-functional *Shaker* K^+ channels, was studied by presenting sequences of dynamically modulated light with a mean contrast of 0.32, close to that of natural sceneries[19], over the range of light intensities to which the photoreceptors are normally exposed (Fig. 1b). The light-induced current, assessed by the bump amplitude, quantum efficiency and macroscopic kinetics (see Methods), was unaffected in *Shaker* mutant photoreceptors. The photoreceptor signal response, $s(t)$, (Fig. 1c, f) and noise, $n(t)$, (Fig. 1d, g) were calculated at each light intensity[20] (see Methods). At all light background intensities, WT flies responded with a larger signal (measured as the signal variance) than Sh^{KS133} flies (Fig. 1i). There was no significant difference in the noise variance between Sh^{KS133} and WT flies over all light intensities ($P < 0.05$). Consequently, the signal-to-noise ratio, SNR(t), of the WT flies was higher than that of the Sh^{KS133} flies over all light backgrounds except the dimmest (Fig. 1j), indicating that the *Shaker* K^+ channels amplify photoreceptor voltage responses.

How much better are WT photoreceptors in gathering information under dynamic, natural-like conditions than their Sh^{KS133} counterparts? To assess performance, we calculated the information capacity, C, of individual photoreceptors over a range of light intensities. Provided that the signal and noise are normally distributed (Fig. 1e, h), the information capacity of the photoreceptor in bits per second can be calculated from the frequency spectrum of the signal-to-noise ratio, SNR(f) (refs 12, 18), using Shannon's formula[21] (see Methods). The SNR(f) increases with increasing light intensity, generating a concomitant increase in the photoreceptor information capacity. A comparison of WT with Sh^{KS133} flies revealed that loss of the *Shaker* K^+ channels reduces the information capacity of the photoreceptors at all but the dimmest light levels, where noise dominates the responses of both cell types (Fig. 2a, b). This information loss was greatest over the lower frequency range of the spectrum (1–50 Hz), both photoreceptor types performing similarly at higher frequencies (50–150 Hz). The frequency distribution of the information depends solely on the $S(f)$ and $N(f)$. Because, under light-adapted conditions, the $N(f)$ of both WT and Sh^{KS133} photoreceptors behaved in a similar manner, the $S(f)$ determines the frequency distribution of the information. To examine the frequency-dependent amplification of the light-induced voltage signal, we calculated the photoreceptor frequency response function, $G(f)$, a measure of the contrast to voltage gain at each frequency[22] (see Methods and Fig. 2c). Responses of WT and Sh^{KS133} photoreceptors show increased contrast gain and broadened bandwidth with increasing mean light intensity; however, the Sh^{KS133} responses contained more high-frequency signals (Fig. 2d).

To explain how loss of the *Shaker* conductance attenuates photoreceptor voltage responses, we developed a mathematical model of the photoreceptor that was based on Hodgkin–Huxley-type equations[23,24], which included *Shaker*, delayed rectifier and leak conductances (see Methods and Supplementary Information). The dynamic properties of the photoreceptor membrane were determined experimentally by injecting white-noise-modulated current. By driving the model with the same stimulus, it was possible to reproduce the WT and Sh^{KS133} membrane behaviour under both dark and light conditions in the time domain (see Methods and Fig. 3a, b). As a further comparison, we calculated first-order Wiener kernels, an approximation of the impulse response of the system, for the experimental and model WT and Sh^{KS133} membranes (Fig. 3c, d). Both the time domain simulations and kernel analysis suggested that the model incorporated the experimentally determined dynamic properties of these membranes. The experimental impedance function (resistance in the frequency domain)

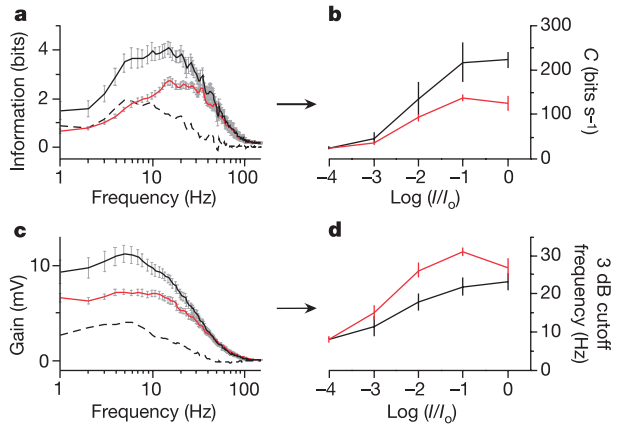

Figure 2 Comparison of the information and gain of wild-type and Sh^{KS133} photoreceptors. **a**, The mean (±s.e.m.) frequency dependence of information extracted from the light-contrast stimulus in WT (black, $n = 21$) and Sh^{KS133} (red, $n = 13$) photoreceptors at background −1. The dashed line is the difference between the WT and Sh^{KS133} photoreceptors. **b**, The information capacity, C (the integral of the information over all frequencies), at five adapting-light backgrounds for both Sh^{KS133} (red) and WT (black) photoreceptors. **c**, The mean (±s.e.m.) frequency response function, $G(f)$, of the WT (black, $n = 21$) and Sh^{KS133} (red, $n = 13$) photoreceptors at background −1. The dashed line is the difference in the gain of the WT and Sh^{KS133} photoreceptors. **d**, The 3 dB cutoff frequency (the point at which the gain falls to half the maximum) increases more rapidly in Sh^{KS133} (red) than in WT (black) photoreceptors as the light intensity increases.

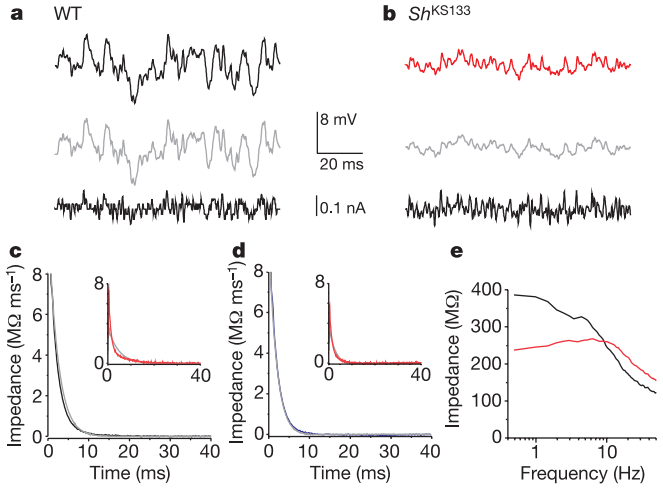

Figure 3 A photoreceptor model predicts accurately the dynamic responses of wild-type and *Shaker* membranes. **a**, Responses of light-adapted WT (upper) and model (middle) membranes to a dynamic current stimulus (peak-to-peak amplitude 0.1 nA) (lower). **b**, Responses of light-adapted *Shaker* (upper) and model (middle) membranes to a dynamic current stimulus (lower). **c**, **d**, First-order Wiener kernels for the WT and model membranes under dark (**c**) and light (**d**) adaptation. The inset shows first-order Wiener kernels for *Shaker* and model membranes under dark and light adaptation (axes are the same as those for WT kernels). **e**, Impedance functions of a WT (black) and a Sh^{KS133} (red) photoreceptor membrane. The Sh^{KS133} impedance function shows reduced gain at low frequencies relative to the WT impedance function.

showed lower impedance in the *Sh*^{KS133} membrane compared with the WT membrane, especially at low frequencies (Fig. 3e). These experimentally determined impedance functions showed similar characteristics to the frequency response function, $G(f)$ (Fig. 2c); the WT membrane had a higher gain than the *Sh*^{KS133} membrane at low frequencies.

Can the properties of the *Shaker* conductance account for the differences between frequency-dependent properties of WT and *Sh*^{KS133} photoreceptors? The overlap of the steady-state activation and inactivation functions of the *Shaker* K^+ channels means that a considerable fraction of these channels are open at the steady-state resting potential, creating a window current[1,24] (Fig. 4a). In addition, the activation–inactivation functions of *Shaker* and delayed rectifier are separated on the voltage scale (Fig. 4a). These two factors produce a voltage range, from −58 to −46 mV, in which the depolarization causes the total steady-state K^+ conductance to decrease (Fig. 4b) because *Shaker* channels inactivate but relatively few delayed rectifier channels are activated. Consequently, the *Shaker* conductance amplifies the voltage signal relative to a non-inactivating K^+ conductance. Is this amplification also present in photoreceptor responses to dynamic stimuli? WT photoreceptor voltage responses were gradually amplified during positive current steps, whereas those of *Sh*^{KS133} photoreceptors were attenuated (Fig. 4c, e). These voltage response characteristics were also successfully predicted by the model (Fig. 4d, f). To elucidate the amplification mechanism, we calculated the time courses of the voltage-activated K^+ conductances in the WT model responses to current steps (Fig. 4g). An increase in the photoreceptor voltage induced by current injection opens further *Shaker* channels that inactivate rapidly, thereby increasing the membrane resistance beyond the resting value, producing a larger voltage response to the same current step.

The frequency range, as seen in the impedance function (Fig. 3e), over which the amplification mechanism is effective is defined by the voltage-dependent inactivation time constant of the *Shaker* K^+ channel. In the voltage range of the photoreceptor responses to white noise current injection, this time constant is comparatively large (~40–100 ms), limiting the amplification to lower frequencies (see Supplementary Information). Therefore, loss of the *Shaker* conductance cannot fully explain the reduction in the *Sh*^{KS133}

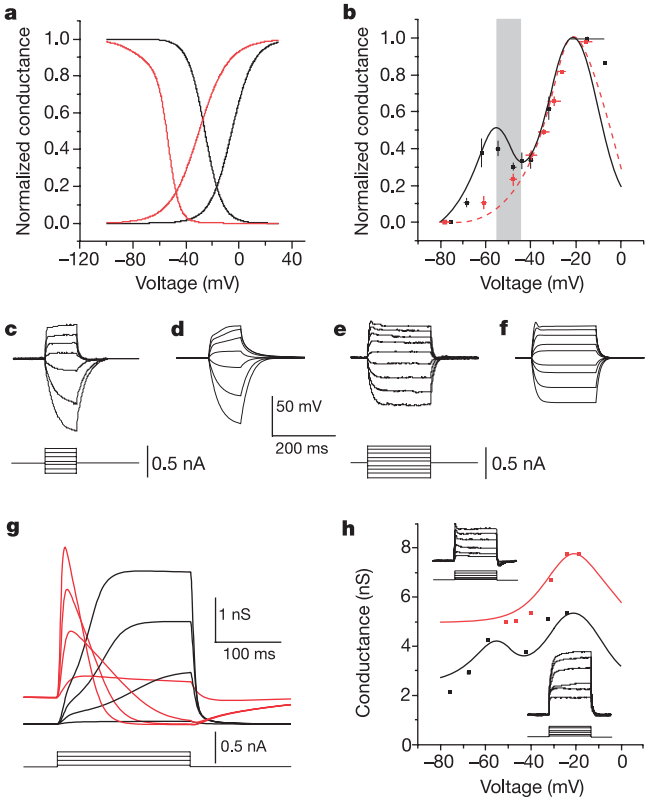

Figure 4 *Shaker*-mediated signal amplification is dependent on the activation–inactivation properties of the *Shaker* and delayed rectifier channels. **a**, Steady-state activation and inactivation curves for the *Shaker* (red) and delayed rectifier (black) conductances used in the model show the overlap of the activation and inactivation properties of the *Shaker* channels, creating a window current at rest. **b**, The normalized steady-state conductance (±s.e.m.) of WT (black squares, $n = 6$) and *Shaker* (red squares, $n = 5$) photoreceptors as a function of membrane voltage, determined by injection of 200 ms current steps. Curves indicate the steady-state conductances predicted by the model for WT (black, solid) and *Shaker* (red, dash) photoreceptors. The shaded area shows the region during which signal amplification occurs due to the voltage separation of the *Shaker* and delayed rectifier channels. **c**, **e**, Intracellular voltage responses of *in vivo* WT (**c**) and *Sh*^{KS133} (**e**) photoreceptors to hyperpolarizing and depolarizing current pulses (maximum 0.38 nA). **d**, **f**, Model simulations of the WT (**d**) and *Sh*^{KS133} (**f**) voltage responses shown in **c** and **d**. **g**, Model simulations were used to resolve the behaviour of the *Shaker* (red) and delayed rectifier (black) K^+ conductances during current pulses in WT photoreceptors. During a current pulse, the *Shaker* conductance inactivates rapidly to below its initial level, boosting the voltage response. **h**, The total steady-state conductance of a WT (black squares) and a *Shaker* (red squares) photoreceptor. The curves show the model predictions of the total steady-state conductance for each photoreceptor. The inset shows the current steps from which the conductances were calculated: *Shaker* photoreceptor, upper left; WT photoreceptor, lower right.

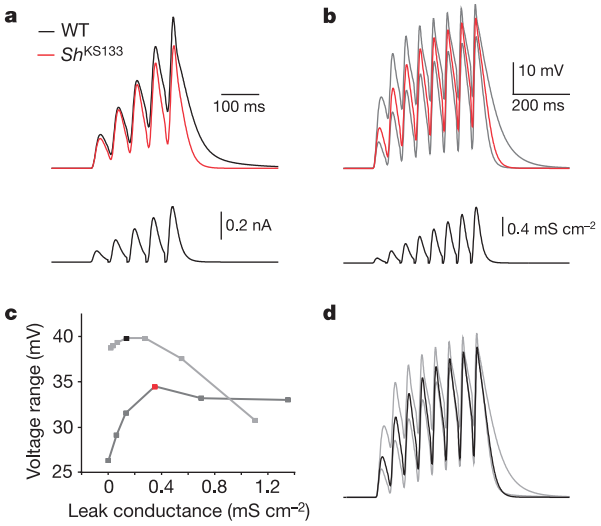

Figure 5 *Shaker* K^+ channel inactivation and the size of the leak conductance contribute to the voltage range of the WT and *Sh*^{KS133} photoreceptors. **a**, Normalized WT (black) and *Sh*^{KS133} (red) model responses to a sequence of five log-normal current pulses (below). **b**, Responses of the *Sh*^{KS133} model membrane (red) and two hypothetical model membranes (dark grey) to a series of log-normal conductance pulses (below). Each hypothetical membrane contained more or less leak conductance than the experimentally determined size of the leak conductance in the *Sh*^{KS133} photoreceptors. The range was taken as the difference between the minimum and maximum peak voltage responses to the conductance stimulus. Although the precise size of the range is specific for the conductance stimulus, the effects of varying the leak will be similar for all saturating stimuli. The stimulus was selected to resemble contrast changes typically observed in natural intensity time series. **c**, The size of the leak conductance in both the WT (grey) and *Shaker* (dark grey) models affects the size of the voltage range. The experimentally determined values for the WT (black square) and *Sh*^{KS133} (red square) photoreceptors maximize the available voltage range. **d**, Responses of the WT model membrane (black) and two hypothetical model membranes (grey) to a series of log-normal conductance pulses (below). Each hypothetical membrane contained more or less leak conductance than the experimentally determined size of the leak conductance in the WT photoreceptors.

photoreceptor impedance at higher frequencies. Indeed, the loss of the *Shaker* conductance would be expected to result in higher resistance at rest; however, Sh^{KS133} photoreceptors had reduced resistances compared with those of WT photoreceptors (Sh^{KS133}, 225.44 ± 25.75 MΩ at −64.3 ± 5.4 mV, $n = 13$; WT, 410.53 ± 34.45 MΩ at −68.1 ± 3.2 mV, $n = 21$). Current pulse experiments showed that the steady-state conductance ($1/R$, where R is resistance) of Sh^{KS133} photoreceptors behaved as would be expected of a WT membrane without *Shaker*, with no further voltage-dependent conductances (Fig. 4b, h). An additional leak is required to model the voltage-independent increase in the Sh^{KS133} conductance compared with that of the WT (Fig. 4h). This leak was larger (~2 nS) than the maximum steady-state *Shaker* conductance (~0.9 nS), but was of the same magnitude as the dynamic *Shaker* conductance in the mid-voltage range of the photoreceptor responses (Fig. 4g). Because of the size of the leak, it cannot be a pure K^+ conductance, which would hyperpolarize the membrane appreciably relative to the WT. To model the experimentally observed resting potential in Sh^{KS133} photoreceptors, two separate leak conductances were required that had reversal potentials of −85 mV (the K^+ equilibrium potential) and −30 mV (obtained by iteration), indicating a K^+ and a Cl^- conductance, respectively (data not shown).

How do the leak conductance and the *Shaker* conductance influence information processing in photoreceptors? The size of the leak conductance affects both the current-to-voltage gain (increasing leak reduces gain) and the spread of a signal across the voltage range. At rest, the *Shaker* conductance effectively acts as a leak conductance, reducing the current-to-voltage gain; however, at higher potentials, *Shaker* channel inactivation increases the gain. Thus, the *Shaker* conductance should increase the spread of the signal across the photoreceptor voltage range. To test this, we drove the model photoreceptors with a series of simulated pulses of light current[12] (Fig. 5a). The amplitudes of the voltage responses of the Sh^{KS133} photoreceptor were compressed compared with those of the WT, indicating that the WT photoreceptors were using the available voltage range more fully than Sh^{KS133} photoreceptors. This leads to a more efficient representation of the vast environmental light variations in the WT voltage range, improving their information processing. The amount of leak conductance cannot compensate for the loss of this amplification in Sh^{KS133} photoreceptors, but scales the amplitude of the voltage responses. Without either *Shaker* or additional leak conductances, photoreceptor voltage responses would also be saturating because of their high gain within a finite voltage range. By driving the model with conductance pulses of successively increasing amplitude, the effects of compression and saturation on the spread of the voltage signal could be seen (see Methods and Fig. 5b). Varying the size of the leak conductance in the model shows that the amount of this conductance present in Sh^{KS133} photoreceptors optimizes the available voltage range (Fig. 5c). Similarly, the amount of leak conductance in the WT photoreceptors is also the optimum for maximizing the voltage range (Fig. 5c, d). This suggests that leak conductance is adjusted in WT photoreceptors to maximize their voltage range and that the additional leak conductance in Sh^{KS133} photoreceptors enables them to compensate partially for the compression and saturation of their voltage range caused by loss of the *Shaker* conductance.

Our results indicate that a reduction in the information capacity of Sh^{KS133} photoreceptors can be explained by loss of the *Shaker* conductance and a compensatory increase in leak conductance. We show that the biophysical properties of *Shaker* channels lead to selective amplification, instead of attenuation[1,14,15], of the graded signals, and to efficient use of the available voltage range. These functions are likely to be widespread in processing graded signals in sensory receptors, and postsynaptic potentials in both vertebrates[2–5,14–17] and invertebrates[9,11,13,16]. In addition, the lower impedance of Sh^{KS133} photoreceptors suggests the presence of a tuning mechanism that compensates the photoreceptors for loss of the *Shaker* conductance, highlighting the dynamic interaction between voltage-activated conductances, neuronal excitability and information coding. Although the details of such a compensation mechanism remain to be determined, there is increasing evidence that neurons may use homeostatic mechanisms to maintain their excitability[25–27]. Such mechanisms are thought to compensate for changing synaptic inputs, but they may also be important for enabling sensory neurons to tune to environmental statistics during development. Our results show both the contribution of specific ion channel properties and the effects of compensatory mechanisms on neuronal information processing. □

Methods

Fly stocks

The WT strain was red-eyed *Drosophila melanogaster* Oregon Red. The null mutation in the *Shaker* channel, Sh^{KS133} (a missense mutation in the core region resulting in non-functional *Shaker* channels[7]), was also expressed in red-eyed flies. Both strains of fly were raised at 19 °C in darkness.

Preparation and electrophysiology

In vivo intracellular recordings were carried out on photoreceptors from flies fixed in a custom-built holder[12]. Recordings were made using quartz microelectrodes filled with 3 M KCl, with resistances between 150 and 220 MΩ. All recordings were made using a switch-clamp amplifier (SEC 10L, npi electronic) in current-clamp mode. The temperature of the flies was maintained at 25 °C throughout the experiments. Photoreceptors were considered for analysis only if their membrane potential was less than −55 mV and they had at least a 45 mV saturating impulse response in dark-adapted conditions. Data acquisition, stimulus generation and signal analysis were carried out using by a purpose-built MATLAB interface[12].

Whole-cell recordings of K^+ currents were made from photoreceptors of dissociated WT or Sh^{KS133} ommatidia[8,9]. Bumps were elicited either by continuous dim illumination or by repeated brief flashes that contained, on average, less than one effective photon, and were detected and analysed off-line using Minianalysis software (Synaptosoft)[28].

Analysis

Single impaled photoreceptors were stimulated with repeated presentations of identical pseudorandom light contrast, $c(t)$ ($= \Delta I/I$, where ΔI is the change in intensity over time and I is the mean intensity over time), generated by a high-intensity green light-emitting diode subtending 1° (Marl Optosource) at five different intensity backgrounds over a range of more than 4 log units up to 3×10^6 photons s^{-1} (ref. 12). Averaging these responses gave the noise-free light-contrast photoreceptor voltage signal[20], $s(t)$, and subtraction of this signal from each individual trace gave the noise, $n(t)$. Dividing $s(t)$ by $n(t)$ gave the signal-to-noise ratio in the time domain, SNR(t). The autospectra of $s(t)$ and $n(t)$—$S(f)$ and $N(f)$, respectively—were calculated using a Fourier transformation. Dividing $S(f)$ by the corresponding $N(f)$ gave the signal-to-noise ratio in the frequency domain, SNR(f). From the SNR(f), the information capacity (bits s^{-1}), C, was calculated using Shannon's formula[21]:

$$C = \int_0^\infty (\log_2[\mathrm{SNR}(f) + 1])\mathrm{d}f$$

After averaging the stimulus and signal, the photoreceptor frequency response, $G(f)$, was calculated by dividing the cross-spectrum of the input (contrast) and output (photoreceptor signal) with the autospectrum of the input[22]. The frequency response, $G(f)$, was then expressed in terms of its gain, the ratio of the photoreceptor response amplitude to the stimulus amplitude[12].

To measure the photoreceptor impedance, a pseudorandom current waveform of small amplitude (<0.2 nA) was injected through the electrode for 10 s to modulate the intracellular photoreceptor voltage. The photoreceptor impedance was calculated in the frequency domain between the average voltage response and the simultaneously recorded current stimulus waveform[12].

Model

A model of the photoreceptors was developed using MATLAB software (The MathWorks) on the basis of Hodgkin–Huxley-type equations[23]. The model incorporated *Shaker* and slow delayed rectifier K^+ conductances (the fast delayed rectifier conductance was omitted because it is present in only some photoreceptors[9]), in addition to K^+ and Cl^- leak conductances. The voltage-dependent parameters (including time constants and steady-state functions for activation and inactivation) for these conductances were obtained either from published data[8,9,29] or from further whole-cell patch-clamp experiments that were performed on isolated photoreceptors (see Supplementary Information). Other photoreceptor membrane properties (the maximum value of the active conductances, the resting potential, leak conductances and membrane capacitance) were estimated from *in vivo* recordings. The voltage-dependent properties of the ion channels, the reversal potentials for each ion and the membrane area were fixed parameters within the model, whereas other parameters were adjusted according to the experimental properties of each individual photoreceptor (see Supplementary Information).

Light channels were modelled as a leak conductance with an equilibrium potential of

+10 mV (see Supplementary Information). The size of the leak was adjusted to produce the same steady-state depolarization in the model as occurred in light-adapted photoreceptors (Fig. 1b). The log-normal shape of the light conductance pulses (Fig. 5) was fitted to experimentally derived light impulse responses[12], and the size of pulses was adjusted so that the largest conductance pulse produced a saturated voltage response with an amplitude similar to that seen in experiments.

To ensure that the Hodgkin–Huxley-type model could be driven with the same dynamic white noise that was used in experiments[30], we tested it by removing the active conductances, thereby reducing it to an analytically solvable RC circuit. A comparison of the model output with the exact solution of the RC circuit in the frequency domain showed that the numerical methods used in the model did not introduce errors. Identical stimuli were used in both modelling and *in vivo* recordings to allow their responses to be compared directly.

Received 1 November; accepted 2 December 2002; doi:10.1038/nature01384.

1. Hille, B. *Ionic Channels of Excitable Membranes* 3rd edn (Sinauer Associates, Sunderland, Massachusetts, 2001).
2. Rudy, B. Diversity and ubiquity of K^+ channels. *Neuroscience* **25,** 729–749 (1988).
3. Coetzee, W. A. *et al.* Molecular diversity of K^+ channels. *Ann. NY Acad. Sci.* **868,** 233–285 (1999).
4. Sheng, M., Liao, Y. J., Jan, Y. N. & Jan, L. Y. Presynaptic A-current based on heteromultimeric K^+ channels detected *in vivo*. *Nature* **365,** 72–75 (1993).
5. Wang, H., Kunkel, D. D., Martin, T. M., Schwartzkroin, P. A. & Tempel, B. L. Heteromultimeric K^+ channels in terminal and juxtaparanodal regions of neurons. *Nature* **365,** 75–79 (1993).
6. Salkoff, L. & Wyman, R. Genetic modification of potassium channels in *Drosophila Shaker* mutants. *Nature* **293,** 228–230 (1981).
7. Kaplan, W. D. & Trout, W. E. The behaviour of four neurological mutants of *Drosophila*. *Genetics* **61,** 399–409 (1961).
8. Hardie, R. C., Voss, D., Pongs, O. & Laughlin, S. B. Novel potassium channels encoded by the *Shaker* gene in *Drosophila* photoreceptors. *Neuron* **6,** 477–486 (1991).
9. Hardie, R. C. Voltage-sensitive potassium channels in *Drosophila* photoreceptors. *J. Neurosci.* **11,** 3079–3095 (1991).
10. Hardie, R. C. & Raghu, P. Visual transduction in *Drosophila*. *Nature* **413,** 186–193 (2001).
11. Weckström, M. & Laughlin, S. B. Visual ecology and voltage-gated ion channels in insect photoreceptors. *Trends Neurosci.* **18,** 17–21 (1995).
12. Juusola, M. & Hardie, R. C. Light adaptation in *Drosophila* photoreceptors: I. Response dynamics and signaling efficiency at 25 °C. *J. Gen. Physiol.* **117,** 3–25 (2001).
13. Laurent, G. Voltage-dependent nonlinearities in the membrane of locust nonspiking local interneurons, and their significance for synaptic integration. *J. Neurosci.* **10,** 2268–2280 (1990).
14. Hoffman, D. A., Magee, J. C., Colbert, C. M. & Johnston, D. K^+ channel regulation of signal propagation in dendrites of hippocampal pyramidal neurons. *Nature* **387,** 869–875 (1998).
15. Magee, J., Hoffman, D., Colbert, C. & Johnston, D. Electrical and calcium signaling in dendrites of hippocampal pyramidal neurons. *Annu. Rev. Physiol.* **60,** 327–346 (1998).
16. Connor, J. A. & Stevens, C. F. Voltage clamp studies of a transient outward membrane current in gastropod neural soma. *J. Physiol. (Lond.)* **213,** 21–30 (1971).
17. Debanne, D., Guérineau, N. C., Gähwiler, B. H. & Thompson, S. M. Action-potential propagation gated by an axonal I_A-like K^+ conductance in hippocampus. *Nature* **389,** 286–289 (1997).
18. de Ruyter van Steveninck, R. R. & Laughlin, S. B. The rate of information transfer in graded-potential neurons and chemical synapses. *Nature* **379,** 642–645 (1996).
19. Laughlin, S. B. A simple coding procedure enhances a neurone's information capacity. *Z. Naturforsch.* **36,** 910–912 (1981).
20. Kouvalainen, E., Weckström, M. & Juusola, M. Determining photoreceptor signal-to-noise ratio in the time and frequency domains with a pseudorandom stimulus. *Vis. Neurosci.* **95,** 1221–1225 (1994).
21. Shannon, C. E. Communication in the presence of noise. *Proc. Inst. Radio Eng.* **37,** 10–21 (1948).
22. Bendat, J. S. & Piersol, A. G. *Random Data: Analysis and Measurement Procedures* (Wiley & Sons, New York, 1971).
23. Hodgkin, A. L. & Huxley, A. F. A quantitative description of membrane current and its application to conduction and excitation in nerve. *J. Physiol. (Lond.)* **117,** 500–544 (1952).
24. Johnston, D. & Wu, S. M.-S. *Foundations of Cellular Neurophysiology* (MIT Press, Cambridge, Massachusetts, 1995).
25. Desai, N. S., Cudmore, R. H., Nelson, S. B. & Turrigiano, G. G. Critical periods for experience-dependent synaptic scaling in visual cortex. *Nature Neurosci.* **5,** 783–789 (2002).
26. Stemmler, M. & Koch, C. How voltage-dependent conductances can adapt to maximize the information encoded by neuronal firing rate. *Nature Neurosci.* **2,** 521–527 (1999).
27. Brickley, S. G., Revilla, V., Cull-Candy, S. G., Wisden, W. & Farrant, M. Adaptive regulation of neuronal excitability by a voltage-independent potassium conductance. *Nature* **409,** 88–92 (2001).
28. Henderson, S. R., Reuss, H. & Hardie, R. C. Single photon responses in *Drosophila* photoreceptors and their regulation by Ca^{2+}. *J. Physiol. (Lond.)* **524,** 179–194 (2000).
29. Hevers, W. & Hardie, R. C. Serotonin modulates the voltage dependence of delayed rectifier and *Shaker* potassium channels in *Drosophila* photoreceptors. *Neuron* **14,** 845–856 (1995).
30. Shampine, L. F. & Reichelt, M. W. The MATLAB ODE suite. *SIAM J. Sci. Comput.* **18,** 1–22 (1997).

Supplementary Information accompanies the paper on *Nature*'s website (http://www.nature.com/nature).

Acknowledgements We thank G. Garcia de Polavieja and H. Robinson for comments on an earlier version of this manuscript. The work was supported by the Royal Society (M.J. and R.C.H.) and the Wellcome Trust (M.J., J.N. and R.C.H.).

Competing interests statement The authors declare that they have no competing financial interests.

Correspondence and requests for materials should be addressed to M.J. (e-mail: mj216@cus.cam.ac.uk).

Ankyrin-B mutation causes type 4 long-QT cardiac arrhythmia and sudden cardiac death

Peter J. Mohler*†, Jean-Jacques Schott†‡, Anthony O. Gramolini*, Keith W. Dilly§, Silvia Guatimosim§, William H. duBell‖, Long-Sheng Song§, Karine Haurogné‡, Florence Kyndt‡, Mervat E. Ali*, Terry B. Rogers‖, W. J. Lederer§, Denis Escande‡, Herve Le Marec‡¶ & Vann Bennett*#

* *Howard Hughes Medical Institute and Departments of Cell Biology, Biochemistry, and Neuroscience, Duke University Medical Center, Durham, North Carolina 27710, USA*
‡ *Laboratoire de Physiopathologie et de Pharmacologie Cellulaires et Moléculaires, INSERM U533, Hôtel-Dieu; and ¶ Département de Cardiologie, Hôspital G&R Laennec, Nantes, France*
§ *Medical Biotechnology Center and Department of Physiology, University of Maryland Biotechnology Institute; and ‖ Department of Biochemistry & Molecular Biology, University of Maryland School of Medicine, Baltimore, Maryland 21021, USA*
† *These authors contributed equally to this work*

Mutations in ion channels involved in the generation and termination of action potentials constitute a family of molecular defects that underlie fatal cardiac arrhythmias in inherited long-QT syndrome[1]. We report here that a loss-of-function (E1425G) mutation in ankyrin-B (also known as ankyrin 2), a member of a family of versatile membrane adapters[2], causes dominantly inherited type 4 long-QT cardiac arrhythmia in humans. Mice heterozygous for a null mutation in ankyrin-B are haploinsufficient and display arrhythmia similar to humans. Mutation of ankyrin-B results in disruption in the cellular organization of the sodium pump, the sodium/calcium exchanger, and inositol-1,4,5-trisphosphate receptors (all ankyrin-B-binding proteins), which reduces the targeting of these proteins to the transverse tubules as well as reducing overall protein level. Ankyrin-B mutation also leads to altered Ca^{2+} signalling in adult cardiomyocytes that results in extrasystoles, and provides a rationale for the arrhythmia. Thus, we identify a new mechanism for cardiac arrhythmia due to abnormal coordination of multiple functionally related ion channels and transporters.

We previously characterized a large French kindred (Fig. 1a) where long-QT syndrome associated with sinus node dysfunction and episodes of atrial fibrillation segregated as an autosomal-dominant trait mapping to an 18-cM interval on chromosome 4q25-27 (ref. 3). Among the 25 affected patients (21 adults and 4 children) included in the study, average rate-corrected QT interval (QTc) was 490 ± 30 ms (for adults) and 465 ± 38 ms (for children) compared with 380 ± 30 ms and 403 ± 36 ms in unaffected individuals. T-wave morphologies characterized by sinusoidal features differed from those observed in the long-QT type 1–3 syndrome (LQT1–3). Sinus node bradycardia or junctional escape rhythm was diagnosed in all patients with LQT4 (ref. 3; see also Supplementary Fig. 1), although 24-h electrocardiogram (ECG) recordings revealed that sinus node dysfunction alternated with normal sinus rhythm. Nine patients were equipped with a rate-responsive atrial pacemaker because of marked bradycardia and the need of beta-blocking therapy. Finally, episodes of atrial fibrillation were diagnosed in 12 adult patients but were absent during childhood. Since the initial description of the family, eight additional individuals have been born. Four were demonstrated to carry the LQT4 haplotype. Sinus node abnormalities were diagnosed *in utero* in all affected members from generation IV.

Present address: Box 3892, Duke University Medical Center, Durham, North Carolina 27710, USA.